Chapter 5
Modeling and structure validation of the artificial cytochrome b

5.1 Introduction

In this chapter, I will describe a procedure how we generated the atomic coordinates of an artificial protein, recently synthesized by Rau and Haehnel (1998) using the template-assembled synthetic strategy. The aim of protein design is to generate novel proteins with tailored structural and functional properties. A four-helix bundle binding two hemes constitutes the catalytical heart of the membrane protein complex Cbc_1 in the respiratory chain and the photosynthetic Cb_6f complex. The model structure mimics the central part of the Cb subunit of the Cbc_1 complex and reproduces a native-like function. It consists of a four-helix bundle, two hemes and a cyclic decapeptide as template. Since no X-ray structure is available, the structural elements of the artificial Cb were assembled from scratch using all known structural informations available and avoiding strain as much as possible. A great deal of work was to generate the coordinates of this protein by stepwise sophisticated modeling techniques. Since the modeling work is extremely technical, only the procedure is given in this chapter and all other details can be found in the Appendix I.

To validate the computer-generated structure of the artificial protein, characteristic observables were calculated and compared with measured quantities. One of these is the redox potential, a key parameter of redox active proteins. The results from the calculation of redox potentials will be discussed in the Chapter 4. The robustness of the model structure is tested by monitoring the conformational stability during a long-term simulation of molecular dynamics (MD) and comparing the results with values obtained from the MD simulations on other proteins with known crystal structure. As suitable native heme protein we considered Cb from the bovine Cbc_1 membrane protein complex, where a crystal structure (Iwata, et al., 1998) is available (Figure 5.1). The RMS deviations from the MD simulations for native and artificial protein are very similar, what demonstrates that the modeled structure of the artificial Cb is relatively rigid and strain-free. In the result section of this chapter, also some structural details of protein and heme conformations of both proteins will be compared.

5.1.1 Protein design

The artificial protein that we studied in detail mimics structure and function of the native Cb. Both, the model protein and the native Cb contain two hemes as cofactors, which are harbored by an anti-parallel four-helix bundle. The helices of the artificial protein are held together by a template. The template is a cyclic decapeptide with anti-parallel β-sheet structure and two β-turns formed by Pro-Gly residues (Rau & Haehnel, 1998). The sequence of the template is given by: *cyclo*(C A C P G C A C P G). The four-helix bundle is formed by two different types of helices, *F* with 29 residues and *G* with 27 residues. The helix *F* contains a phenylalanine at position 15. Helix *G* contains glycines at positions 8 and 22, where helix *F* contains histidines. Their sequences are closely related to the sequence of helices from

Rhodobacter captulatus, as well as to the sequence of the Maquette designed by Robertson et al. (1994) to form the four-helix bundle (see Appendix G). The sequences of helices *F* and *G* are given below:

helix *F*:

N-terminus (at template of Cb) C-terminus (at open end of Cb)

	1	2	3	4	5	6	7	8	9	0	1	2	3	4	5	6	7	8	9	0	1	2	3	4	5	6	7	8	9	
BrAc	G	G	E	L	R	E	L	H	E	K	L	A	K	Q	F	E	Q	L	V	K	L	H	E	E	R	A	K	K	L	NH_2

helix *G*:

N-terminus (at open end of Cb) C-terminus (at template of Cb)

	1	2	3	4	5	6	7	8	9	0	1	2	3	4	5	6	7	8	9	0	1	2	3	4	5	6	7	
Ac	L	E	E	L	W	K	K	G	E	E	L	A	K	K	L	Q	E	A	L	E	K	G	K	K	L	A	K	NH_2
																											|	
																											BrAc	

(underlined residues are conserved in sequences of Cb from different species)

A model structure of the artificial Cb is displayed in Figure 5.2. It consists of two pairs of identical helices, F_1, F_2 and G_1, G_2, which form the four-helix bundle. Two hemes are bound by the histidine residues of the parallel helices F_1 and F_2, which alternate in the bundle with the anti-parallel helices G_1 and G_2. The binding helix *F* is modeled with two heme-ligating histidines separated by 13 residues, with a central phenylalanine and two arginines at a distance of three amino acids away from the histidines. In the shielding helix *G*, two glycines were positioned at the same height as the ligating histidines in helix *F* to provide space for a tight packing of the heme edges. To avoid charged end groups and to increase stability of the helices, the C-termini are amidated (NH_2) and the N-termini are acetylated (Ac). This arrangement of the synthetic four-helix bundle protein was fixed by a template with four cysteines that bind the helices via bromoacetylated groups (BrAc) attached to two N-terminal glycines and two side chain of the C-terminal lysines of the heme-binding *F* and shielding *G* helices, respectively. Hence, the helices are connected by thioether bonds with the cysteines of the template.

The hemes are situated in the hydrophobic binding core of the four-helix bundle and axially coordinated by histidines belonging to two oppositely placed *F* helices. The heme planes are in parallel orientation. The propionic (PR) groups of both hemes point to the nearest helix ends as in the native Cb. The arginine residues at positions 5 and 25 of helix *F* provide positive charges near the position of the PR groups of the hemes, what enables the formation of salt bridges between them. To isolate the two hemes and to fill the hydrophobic space between them, there is a phenylalanine at residue position 15 in the center of helix *F*. In the native structure the helices terminate close to the edge of the heme groups and the binding pocket is shielded against the hydrophilic phase by loops connecting the helices on both sides of the membrane. In the model structure the helices are longer and the shielding of the hydrophobic interior may be provided by tryptophans in position 5 of the helices *G* at one end and by the template at the other end of the synthetic Cb molecule.

Except of the four histidines, the artificial protein conserves the interior packing of the hemes by hydrophobic residues. The formation of the four-helix bundle is driven to a great extent by the resulting hydrophobic interactions. The residues situated on the outer surface of the helix bundle are hydrophilic to increase solubility and possibly to stabilize the helices by salt bridges between lysines and glutamates at the solvent-exposed surface. All of that one can clearly see from the helical wheel representation in figure 5.3. As a result one obtains a water soluble model protein, where the anti-parallel helices shield the heme binding pocket.

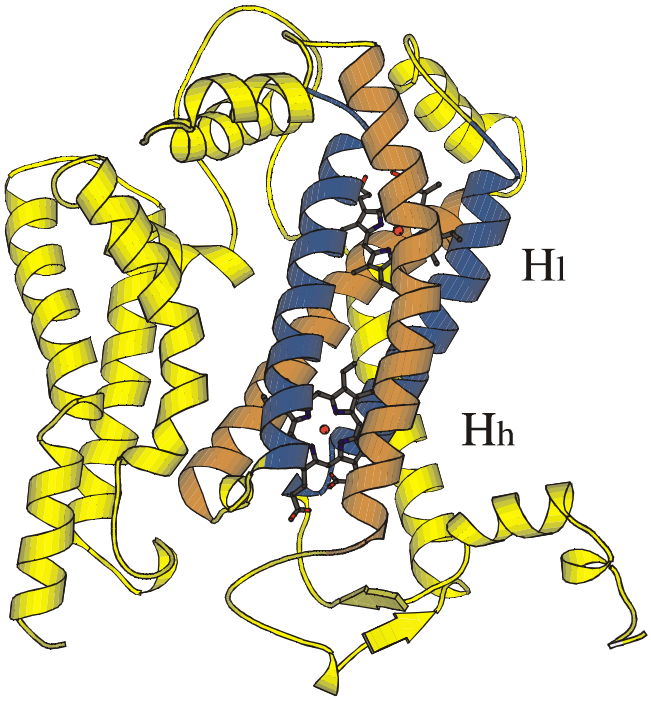

Figure 5.1: Crystal structure of the C chain of the cytochrome bc_1 complex from bovine heart (Iwata et al., 1998). The four-helix bundle embedding the two hemes is displayed in blue and orange color. The four-helix bundle of the native Cb is displayed in the same orientation as the artificial Cb (see Fig. 5.2). The two helices corresponding to the helix of type *G* in the artificial Cb are shown in blue, the other two helices of the bundle corresponding to the helices of type *F* are in orange. The low potential heme H_l is in the upper part, the high potential heme H_h is in the lower part of the figure.

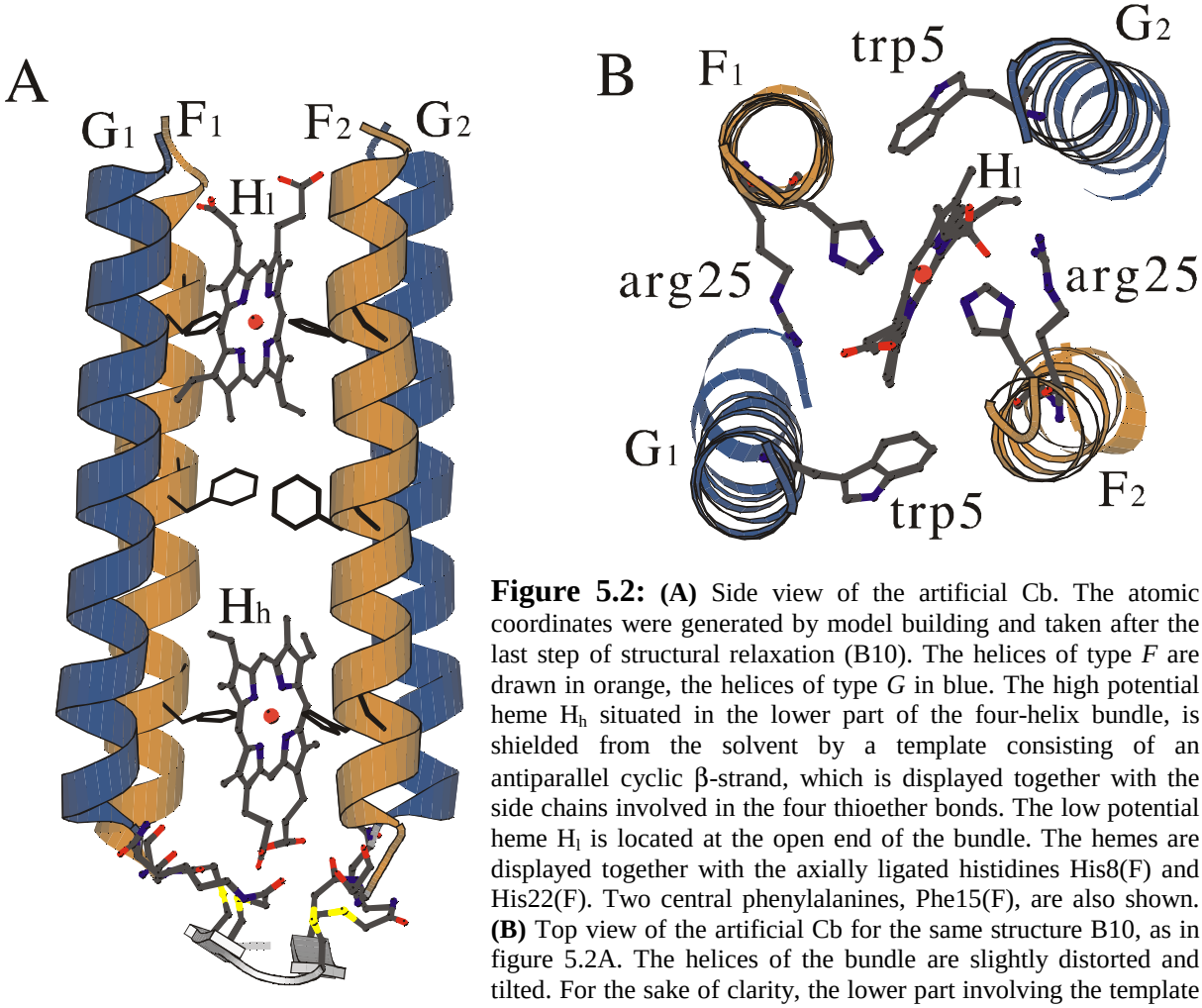

Figure 5.2: **(A)** Side view of the artificial Cb. The atomic coordinates were generated by model building and taken after the last step of structural relaxation (B10). The helices of type *F* are drawn in orange, the helices of type *G* in blue. The high potential heme H_h situated in the lower part of the four-helix bundle, is shielded from the solvent by a template consisting of an antiparallel cyclic β-strand, which is displayed together with the side chains involved in the four thioether bonds. The low potential heme H_l is located at the open end of the bundle. The hemes are displayed together with the axially ligated histidines His8(F) and His22(F). Two central phenylalanines, Phe15(F), are also shown. **(B)** Top view of the artificial Cb for the same structure B10, as in figure 5.2A. The helices of the bundle are slightly distorted and tilted. For the sake of clarity, the lower part involving the template and the high potential heme is not shown. The low potential heme H_l is displayed together with the axially ligated histidines His22(F_1) and His22(F_2) and the two arginines Arg25(F) forming salt bridges with the PR groups. Furthermore, the two tryptophanes Trp5(G_1) and Trp5(G_2) shielding the low potential heme at the top of the four-helix bundle from the solvent are shown.

5.2 Methods

5.2.1 Generation of atomic coordinates

A crystal structure of the artificial Cb consisting of 2218 atoms is not available yet. Nevertheless, we were able to construct atomic coordinates of this model protein, since many structural details are very well defined. The generation of coordinates of the artificial protein by modeling techniques and constrained energy minimization was done using the program CHARMM (Brooks et al., 1983; MacKerell et al., 1998). The procedure that we used, allows to repeat individual modeling steps in order to optimize the resulting structure. The atomic coordinates of the model structure obtained after the last step of structural relaxation are available from the web-site address:

http://lie.chemie.fu-berlin.de/papers/cb1.html.

To generate atomic coordinates of a stable model structure of the artificial Cb required many attempts. When we observed large conformational changes after applying energy minimization to relax strain from the model structure, we discarded these structures. We varied the modeling steps iteratively to avoid strain in the model structure before we even applied steps of structural relaxation. We found that the stepwise constrained energy minimization is crucial to get finally a reliable and stable model structure. If one directly performs the energy minimization without any constraints or MD simulation on a molecular structure that is under strain, the well prepared structural details could get lost, or even worse the structure may literally explode. Therefore, we used different types of constraints during the various steps of the structural relaxation to stabilize specific features of the molecular structure. Here, I will only give a short overview of the modeling and minimization steps that we applied. The code given in brackets refers to the corresponding steps described in more detail in Appendix I.

In the first seven modeling steps we generated the atomic coordinates of the four helices (A1,A2), the two hemes (A4, A5) and the cyclic decapeptide (A6, A7) and assembled them to form the complete model of the artificial Cb as faithful as possible without using structural relaxation. The imidazole rings of the four axially ligated histidines, were appropriately reoriented by resetting the torsion angles and patched to the hemes (A3). The cyclic decapeptide was patched to the four helices via thioether bonds between four cysteines of the decapeptide and acetylated N-terminal Gly1 of the helices *F* or acetylated side chains of the C-terminal Lys27 of the helices *G* (A7).

After the model building, the structure of artificial protein is still under the strain and has packing problems particularly with respect to the side chains. The strain and van der Waals clashes were removed by applying constrained energy minimization using the force field of CHARMM22 parameter set (MacKerell et al., 1998). At the beginning of the structural relaxation we applied several harmonic constraints to the heme-imidazole torsion angles to keep the imidazole planes orthogonal to the heme plane. These constraints were left until the last steps (B10) of minimization. First, the side chains of the four histidines were energy minimized with appropriate constraints (B1). Then, the conformations of the arginines involved in salt bridges with heme PR groups were adjusted by constraint energy minimization (B2). Next, we minimized the side chain conformations of the two phenylalanines dividing the hydrophobic core of the four-helix bundle (B3). Now all side chains were relaxed by energy minimization except the atoms of arginines, phenylalanines and cysteines (B4). Namely, we wanted to keep them in their present conformation and to adjust the positions of all other side chains. After that we could relax all side chains together

(B5). Then the cyclic decapeptide was energy minimized (B6, B7). In the following minimization steps also the hemes were relaxed. First, we simultaneously relaxed the conformations of the propionic acids and arginines forming salt bridges with each other (B8). Then, we relaxed the artificial Cb as a whole by gradually reducing the constraints applied to the peptide backbone atoms (B9). Finally, the resulting model structure was energy minimized without any constraints (B10).

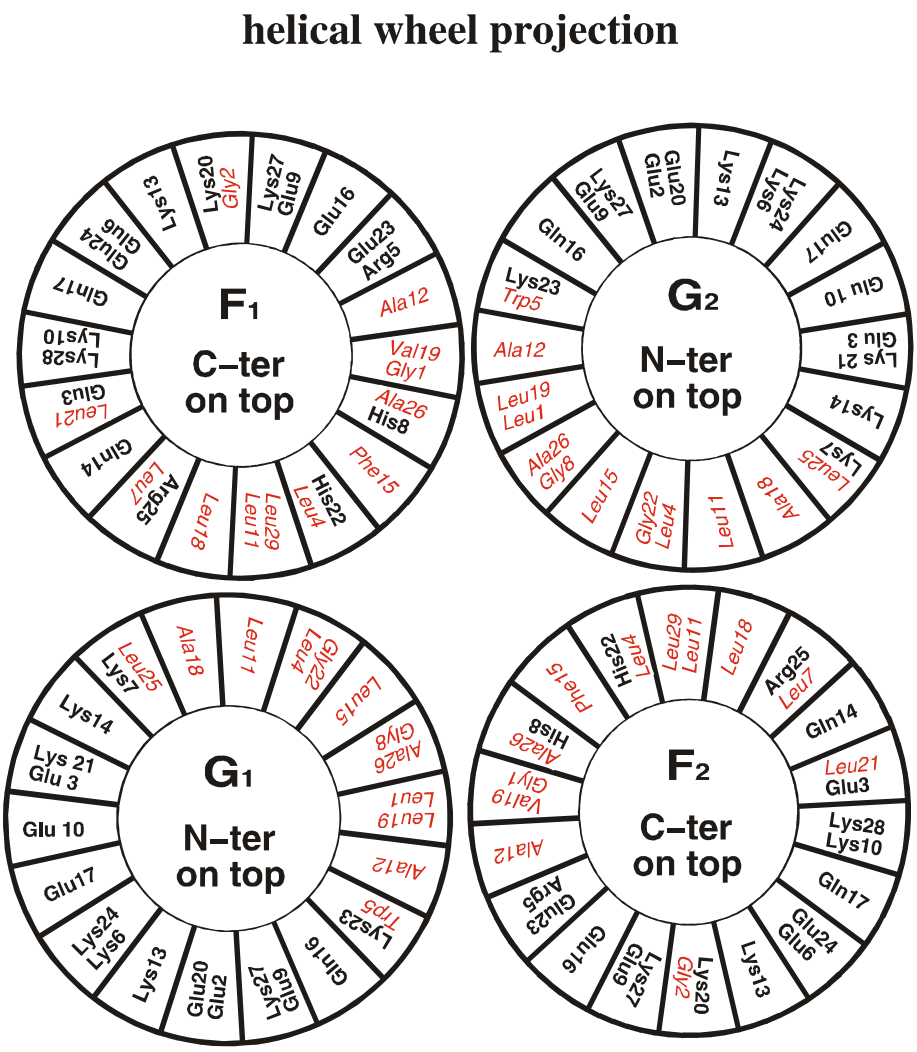

Figure 5.3: Helical wheel projection of the artificial four-helix bundle viewed from the top. Hydrophobic residues are given in red color, hydrophilic residues by black symbols. Besides the four histidines, only hydrophobic residues are pointing toward the center of the four-helix bundle, thus facilitating the association of the four helices to the helix bundle. On the surface of the bundle nearly all residues are hydrophilic, which improves the solubility of the artificial Cb. The helices of type *F* and *G* correspond to the helices denoted H_1 and H_2 by Rau and Heahnel (1998), respectively.

5.2.2 Preparation of the native Cb chain for MD simulation

We used the crystal structure of the mitochondrial Cbc_1 complex from bovine heart, which was solved at 100 K and pH = 6.6 at a resolution of 3.0 Å (Iwata et al., 1998; PDB code 1BE3). For the MD simulation only the Cb subunit (chain C in PDB entry) containing two hemes was considered. The titratable groups were considered to be in their standard protonation state, during the MD simulation. Hydrogen atoms were added to the X-ray structure with the HBUILD command of CHARMM22, leading to an all atom representation. The total number of atoms of the Cb subunit including all hydrogens and two hemes is 6242. The hydrogen atom positions were subsequently energy minimized with the CHARMM22 force field, keeping all non-hydrogen atoms fixed. To provide equivalent starting conditions for MD simulation between the native and artificial Cb, the structure of the native Cb was relaxed in similar fashion. First, all side chain atoms were energetically minimized, while both hemes and backbone atoms were fixed. Then, the whole structure of the native Cb was energetically minimized without applying constraints.

5.2.3 Molecular dynamics simulation

To test the stability and lack of strain in the resulting model structure we performed an MD simulation of the artificial protein and for comparison also for the native Cb subunit of bovine heart (Iwata et al., 1998). For that purpose, we ran Langevin dynamics simulation with a friction coefficient of $\beta = 5.0\ ps^{-1}$ in vacuum at a temperature of T = 300K, which was reached after 15 ps for the artificial Cb and after 10 ps for the native Cb. To avoid fast heating and strong coupling between the molecular system and a heat bath, the friction mechanism was applied only to the C_α atoms. The length of covalent bonds involving hydrogen atoms were constrained with the SHAKE algorithm (Ryckaert et al., 1977), so that the time propagation could be done in 1-fs steps. Coulomb and Lennard-Jones (van der Waals) interactions of each atom were calculated with the group switch cut-off scheme (Brooks et al., 1983). At distances of less than 9.0 Å the full atom pair interactions are applied, from 9.0 to 10.0 Å the potential gradually diminishes, and at distances larger than 10.0 Å atom pair interactions vanish. As a cut buffer radius, we used the value of $r_{cutbuff} = 12.0$ Å. The value of the dielectric constant was $\varepsilon = 1$ everywhere. The trajectories have a length of 1000 ps. Atomic coordinates were stored each 100 fs yielding 10000 coordinate frames. We considered the last 700 ps of the trajectories to compute averages.

5.3 Results and Discussions

5.3.1 Structural relaxation of the artificial cytochrome b

As it was mentioned in method section and in very detail explained in Appendix I, we built up the model structure and carefully relaxed it in 13 discrete minimization steps by gradually reducing the constraints. We monitored the changes in the root mean square (RMS) deviations for different parts of the structure, to see how subsequent modeling and relaxation steps improve the model structure. These data are collected in Table 5.1, which provides RMS deviations between the final completely relaxed model structure (B10) and the different partially relaxed structures (X). RMS deviations between initial the non-relaxed model

structure (A7) and the final completely minimized model structure are 1.5Å, what is a typical value obtained by energy minimization of the crystal structure of a protein in vacuum. It already shows a good quality of our initial model structure (A7). The RMS deviations gradually decrease through individual minimization steps. From Table 5.1, one can also see that template atoms were not moved before relaxation step B4, backbone atoms of the helix bundle not before step B6 and atoms of the hemes not before step B8. In step B9, the harmonic constraints applied on the backbone atoms were gradually reduced, to avoid large conformational changes that can destroy carefully modeled structural details. Hence, the table 5.1 illustrates how the model structure is improved and RMS deviations become smaller, going from one to the next step during the energy minimization procedure.

Starting from the ideal planar conformation of the hemes, the heme conformations are changed through the energy minimization steps, and table 5.2 shows these changes by the RMS deviations. The heme atoms were not moved before the step B8, where only the atoms of the PR groups were relaxed. After reducing the constraints applied to two hemes, their conformations became slightly different through the process of structural relaxation (Table 5.2). The RMS deviations between all atoms of the two hemes are 1.0 Å after the last step of minimization and 1.2 Å in the average structure of MD simulation. Of course, the RMS deviations of porphyrin rings are much smaller.

5.3.2 Salt bridges in the artificial Cb

We assumed that an acidic and basic residue pair forms a strong salt bridge, if the corresponding oxygen-hydrogen distance is less than 4 Å. Since the salt bridge interactions are of the electrostatic nature, namely the long-range interactions between the two oppositely charged residues, this is an reasonable estimation. All four PR groups from the two hemes form strong salt bridges inside of the hydrophobic binding pocket with four arginines. Thereby, the arginines Arg5(F_1), Arg5(F_2), Arg25(F_1), and Arg25(F_2) form salt bridges with PRA(H_h), PRD(H_h), PRA(H_l), and PRD(H_l), respectively. The corresponding O–H distances between the PR groups and the arginines are 2.4Å, 1.6Å, 2.1Å, and 1.5Å. From the many possibilities to form salt bridges between glutamates and lysines on the outer helix surfaces, our model of the artificial Cb exhibits only four strong salt bridges. These salt bridges are formed by the residue pairs: Glu16(F_2)–Lys13(F_2), Glu24(F_2)–Lys28(F_2),Glu20(G_2)–Lys24(G_2) and Glu10(G_1)–Lys14(G_1). Their corresponding oxygen-hydrogen distances are 2.9Å, 1.7Å, 2.4Å, and 3.8Å, respectively. This is astonishing, since the CHARMM22 energy function used to model the atomic coordinates was applied under vacuum conditions, where electrostatic interactions involving salt bridges on a protein surface should be overestimated. One can expect many more possible salt bridges. There are two possible explanations why only four of them appear in our model structure. First, almost each Lys or Glu has two possible partners for making the salt bridge, what can cause that mutal distances between each acid-base pair are a little bit larger after the energy minimization, as a compromise between two possibilities. Secondly, the side chain of Lys is longer than the side chain of Glu and when they are on the top of each other, Lys side chain has to adopt probably energetically less favorable bent conformation, to be able to form a salt bridge with Glu. From experiment it is known that solvent exposed salt bridges are generally only marginally stable, since in the high dielectric medium of aqueous solution these interactions are screened very efficiently.

Table 5.1: RMS deviation in Å between structures of the different modeling steps and the final structure of the artificial Cb. The RMS deviations are calculated by superimposing the final model structure (B10) after all steps of energy minimization with the structures obtained after individual steps of structural relaxation (X = A7, . . . $B9_5$) using the Kabsch algorithm (Kabsch, 1976, 1978). The steps of structural relaxation are explained in the Appendix I. Step B9 consists in five individual steps of energy minimization using constraining forces of decreasing strength.

X – B10	all atoms	backbone atoms	Side chains	4-helix bundle	template atoms	heme H_l	heme H_h
X = A7	1.536	0.877	1.718	1.555	1.073	0.545	0.874
X = B1	1.527	0.877	1.707	1.547	1.073	0.545	0.874
X = B2	1.483	0.877	1.651	1.496	1.073	0.545	0.874
X = B3	1.477	0.877	1.644	1.489	1.073	0.545	0.874
X = B4	1.067	0.877	1.128	1.042	0.969	0.545	0.874
X = B5	1.050	0.877	1.108	1.023	0.950	0.545	0.874
X = B6	1.023	0.816	1.090	1.023	0.564	0.545	0.874
X = B7	0.994	0.790	1.057	1.002	0.436	0.545	0.874
X = B8	0.988	0.790	1.049	1.000	0.436	0.480	0.831
X = $B9_1$	0.949	0.784	1.004	0.965	0.436	0.440	0.571
X = $B9_2$	0.889	0.742	0.937	0.900	0.430	0.405	0.571
X = $B9_3$	0.691	0.614	0.716	0.691	0.422	0.365	0.553
X = $B9_4$	0.478	0.412	0.499	0.472	0.396	0.322	0.409
X = $B9_5$	0.177	0.173	0.179	0.163	0.356	0.121	0.138

Table 5.2: RMS deviation in Å between the two hemes in artificial Cb for the different steps of modeling. The RMS deviations were calculated using the Kabsch algorithm (Kabsch, 1976, and 1978) by superimposing the structure of the actual modeling step with the initial structure before modeling step B8.

modeling step	all atoms [a]	porphyrin ring
B8	0.380	0.000
$B9_1$	0.790	0.222
$B9_2$	0.801	0.213
$B9_3$	0.784	0.203
$B9_4$	0.954	0.320
$B9_5$	1.021	0.285
B10	1.010	0.386
average from MD	1.239	0.321

[a] All atoms including the atoms of the propionate groups

5.3.3 Comparison of heme conformations in artificial and native Cb

The heme conformation, the type and orientation of axial ligands and their interactions with the heme and with the protein environment are crucial for the values of the redox potential in the heme-proteins. Therefore, in following I will compare the structural differences, particularly related with the histidine–heme conformations in the X-ray structure of the native Cb (Iwata et al., 1998) and in the artificial Cb obtained by modeling procedures. The corresponding structural data are collected in Table 5.3. In the native Cb, the Nε2–Fe bond lengths vary for the crystal structure, the energy minimized structure and the average of the MD simulation only between 1.98Å and 2.08Å, which is close to the ideal value of 2.05Å assumed in the CHARMM22 force field. In the artificial Cb, these bond lengths are slightly larger varying between 2.10Å and 2.23Å. They remain somewhat larger even after the MD simulation. This may be a hint of some steric interactions in the artificial Cb, which prevent the helices of type *F* to come closer to the heme.

The Nε2–Fe–Nε2' bond angles involving the imidazole nitrogen atoms bound to the heme iron exhibit deviations of about $\pm 10^0$ from its ideal value of 180^0, except for the angle involving His83 and His182 of the native Cb with a deviation of almost 30^0. But, after energy minimization, that deviation diminishes. The idealized histidine-heme coordination assumes the orthogonality of the imidazole ring and the heme plane. Hence, the angle between the normal of the heme plane and the normal of the axially ligated imidazole plane should be about 90^0. The largest deviation of 21.5^0 from 90^0 can be observed for His83 in the crystal structure of the native Cb, which decreases after energy minimization. Deviations of these angles are generally less pronounced for the artificial Cb, probably because this structure is relaxed by energy minimization more extensively. The angle between the heme plane normal and the vector in the imidazole plane pointing from Nε2 to the midpoint of Cγ and Nδ1 (see Fig. 4.1) characterizes the inclination of the imidazole plane with respect to the heme plane in a direction orthogonal to the imidazole plane normal. Due to steric effects also this angle should be close to 0^0 or 180^0 depending on whether the considered imidazole plane is above (as in Fig. 4.1) or below the heme plane, respectively.

The torsion angles α, β, and γ defined in figure 4.1, describe the orientation of the imidazole ring plane with respect to the PR groups of the heme, with respect to the histidine backbone and the position of the histidine backbone relative to the heme, respectively (Zarić et al., 2001). For idealized imidazole-heme geometry, the three torsion angles are related to each other ($\gamma = \alpha + \beta$), as it was pointed out in Chapter 4. The deviations from this relation encountered here are in the range of only $\pm 5^0$ (see Table 5.3). Analyzing the histidine-heme conformations in the model protein, one can see that all angles β are in the allowed regime of about $\pm 90^0$. In case of the histidines ligated to the heme H_l, the backbone–heme orientation prevents the favorable orientation of the imidazole rings towards the PR groups, while that is not the case with the histidines of the heme H_h, which roughly point towards the corresponding PR group that is at the same side of the heme plane as the imidazole ring.

The relative orientation of the two hemes can be measured by the angles between the vectors CHA–CHC (and CHB–CHD) (see Fig. 4.1) belonging to different hemes. These angles are close to zero for the artificial Cb indicating that the heme planes are mutually parallel and that the PR groups point nearly exactly in opposite directions (see Table 5.4). That reflects the regularity in the structure of the artificial Cb, where the helix axes are not so much tilted even after MD simulation. In the native Cb, the helices are very much tilted and even bent due to the presence of proline residues in the sequence of the helices αC (Pro134) and αD (Pro186), and a glycine in the helix αB (Gly86). Consequently, the relative orientation of the hemes is also less regular.

Table 5.3: Conformation of the hemes in the native and artificial cytochrome b.

	Fe-Nε2 distance (Å)	Nε2-Fe-Nε2' angle [c]	heme and – His normal angle [d]	heme normal - Nε2-middle angle [e]	torsion angle α[f]	torsion angle β[f]	torsion angle γ[f]
native Cb [a]							
His83	2.08	152.1	68.5	155.8	136.1	-17.4	120.2
	2.06	177.0	82.8	171.6	161.5	-42.3	110.6
	2.03	171.9	95.8	163.0	166.2	-67.0	103.8
His182	2.06		107.1	17.6	112.8	65.6	-168.4
	2.07		83.7	6.4	63.4	106.4	-180.0
	1.98		87.2	9.7	68.9	118.0	-168.0
His97	2.08	171.1	81.5	167.6	5.1	-37.8	-37.1
	2.00	167.8	87.7	177.3	49.5	-83.2	-44.3
	2.07	169.0	108.9	173.6	60.0	-85.0	-39.6
His196	2.06		84.9	9.6	-87.3	72.6	-6.6
	1.99		92.4	7.8	-69.7	62.2	5.9
	2.07		73.2	22.7	-34.2	60.9	34.1
artificial Cb[b]							
His22(F_1)	2.22	172.1	94.6	161.4	105.2	-101.4	-12.7
	2.11	171.1	91.4	156.6	87.3	-59.9	21.1
His22(F_2)	2.23		78.5	21.3	-120.2	124.1	12.7
	2.21		77.9	4.6	-109.3	93.7	16.6
His8(F_1)	2.17	174.1	107.3	159.2	-45.8	-86.5	-138.9
	2.19	171.6	108.6	163.8	-46.0	-71.0	-121.0
His8(F_2)	2.12		91.2	19.5	86.3	94.0	179.4
	2.10		84.2	13.8	82.5	75.0	168.4

[a] Top values are from the crystal structure of the native Cb; middle values are from the energy minimized X-ray structure of the native Cb; bottom values in brackets are averages from MD simulations.
[b] Top values are from the minimized structure of the artificial Cb; bottom values are averages from MD simulations.
[c] The bond angle Nε2-Fe-Nε2' refers to pairs of histidines axially ligated to the same heme. For the native Cb, the first triplet of values corresponds to the pair His83–His182 and the second triplet of values to His97–His196. For the artificial Cb, the first doublet of values corresponds to His22(F_1)–His22(F_2) and the second doublet of values to His8(F_1)–His8(F_2). Footnote a and b are valid correspondingly.
[d] The vectors Fe-NA, Fe-NB of the heme and the heme normal form a right handed coordinate system. The same is the case for the vectors Cγ-Cδ and Cγ-Nδ1 of the histidine and the imidazole ring normal.
[e] The inclination of the axially ligated imidazole ring with respect to the heme plane is measured by the angle of the heme plane normal with the vector going through atom Nε2 and the midpoint of the Cγ-Nδ1 bond (see Fig. 4.1).
[f] For a definition of the torsion angles α, β, and γ see Fig. 4.1.

Table 5.4: Relative orientation of hemes in native and artificial Cb.

angles [a]:	CHC(H_l)-CHA(H_l) with CHA(H_h)-CHC(H_h)	CHB(H_l)-CHD(H_l) with CHD(H_h)-CHB(H_h)
native Cb [b]	38.2	41.0
	36.8	36.9
	33.7	35.1
artificial Cb [c]	5.0	3.8
	8.9	-14.8

[a] Angles are given in degrees. [b] Top values are from the crystal structure of the native Cb; middle values are from the energy minimized X-ray structure of the native Cb; bottom values are averages from MD simulations. [c] Top values are from the minimized structure of the artificial Cb; bottom values are averages from MD simulations.

The binding situation of hemes incorporated into the model protein was recently investigated by EPR and ENDOR spectroscopy (Fahnenschmidt et al., 1999), as well as by Mössbauer and EPR spectroscopy (Iakovleva et al., submitted). The EPR spectra show the occurrence of two types of the hemes. The Fe^{3+} low-spin signal refers to the bis-histidine ligated heme with approximately parallel histidine planes, which would correspond to the low potential heme near the open end of the four-helix bundle. The second contribution corresponds to a highly anisotropic low-spin Fe^{3+} (HALS) species. It is characteristic of bis-histidine ligation with tilted or twisted imidazole planes, and can be assigned to the high potential heme on the template side. Also the distance of axial histidines from the metal center and their mutual orientation was studied by ENDOR spectroscopy. However, this method allows only conclusions based on a comparison with the related situations in native proteins or model complexes, where the imidazole orientation and corresponding distances are known. Our model of the artificial Cb roughly agrees with these experimental results. The histidine orientation is approximately parallel for the H_l heme (16^0), while it is more perpendicular for the H_h heme (48^0). However, both hemes possess histidines with planes that are tilted relative to the heme plane such that the corresponding distances Fe–Hε1 and Fe–Hδ2 are not equal. Such an asymmetry is also not unusual for the native Cb structures (1be3 and 1bcc). The positions and orientations of the axially ligated histidines in the artificial Cb are obtained by energy minimization using the CHARMM22 force field where we did not apply any additional energy term, which would constrain the Fe–Hε1 and Fe–Hδ2 distances and enforce symmetric orientation.

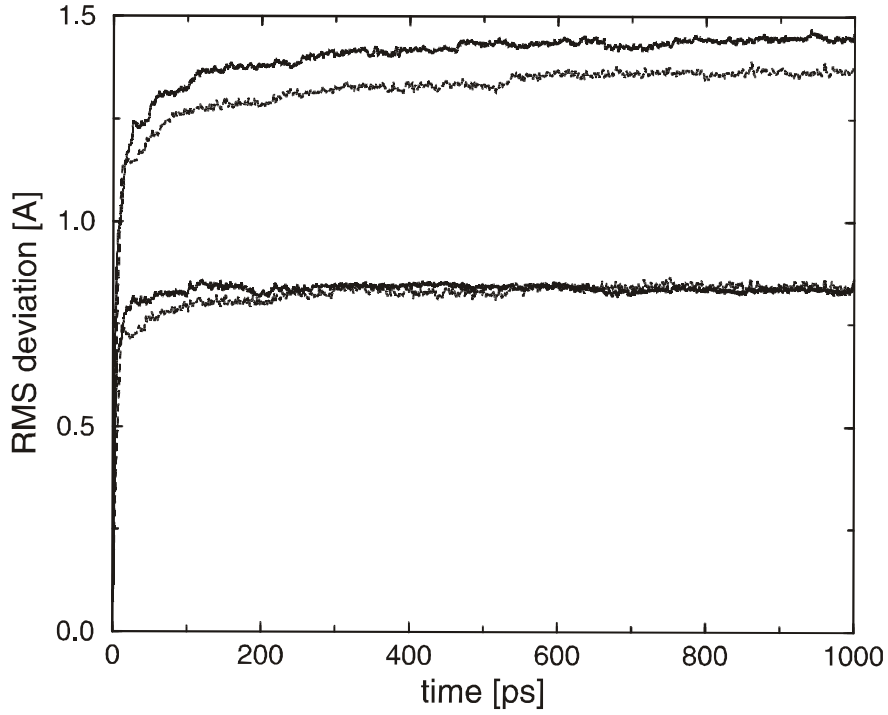

Figure 5.4: Time evolution of the RMS deviations for the artificial and native Cb. To demonstrate the stability of the structures from the artificial and native Cb, the RMS deviations are displayed as a function of time for 1 ns. The RMS deviations of the backbone atoms without hemes (lower pair of curves) and of all atoms (upper pair of curves). The curves with the slightly smaller values are the data from the native Cb. To remove short time fluctuations in the RMS deviations, averages over 2 ps corresponding to 20 sets of coordinates were displayed. For more details see text.

5.3.4 Stability of the artificial and native Cb

The robustness of the model Cb structure is tested by monitoring the conformational stability during a long-term simulation of molecular dynamics (MD) and comparing the results with the MD simulation of the native Cb from the bovine Cbc_1 complex, where a crystal structure (Iwata et al., 1998) is available. The dynamics simulations were done in vacuum. The trajectories have a length of 1000 ps. The conditions of the MD simulations are given in section 5.2.2 and 5.2.3. Figure 5.4 exhibits the time dependence of the RMS deviations for the X-ray structure of the native Cb and completely energy minimized structure of the artificial Cb. Two pairs of lines are depicted in that figure. The upper curves display the RMS deviations of all atoms for the native and artificial protein structure. The lower pair refers to the backbone atoms of the four-helix bundle and template only. After 100 ps the RMS deviations of the backbone atoms reach a value of 0.85 Å and practically do not increase any more. The RMS deviations of all atoms reach a plateau value of 1.45 Å for the artificial Cb and 1.34 Å for the native Cb. The RMS deviations from the MD simulations for native and artificial protein are very similar, what demonstrates that the modeled structure of the artificial Cb is relatively rigid and strain-free.

Obtained RMS deviations are typical for MD simulations under vacuum conditions applied to crystal structures of relatively stable proteins. Hence, in that respect the model structure of the artificial Cb may be as good as a crystal structure. Furthermore, the average structure as well as the structure of the artificial Cb after 1 ns of MD simulation remain all structural details as a model structure. For instance, the helices essentially retain their secondary structure, as in agreement with the results of the circular dichroism measurements that estimate the helicities of 81% for the whole structure (Rau & Heahnel, 1998). The value based on the modeling is 89%. We observed that the values of the template torsion angles exhibit relatively large fluctuations, but still we could distinguish two β-strands and two turns. However, variations from the ideal conformation angles of cyclic peptides by as much as 30^0 are also common for native proteins (Voet & Voet, 1995). All these observations are in a favor of a relative stability of the artificial Cb. Comparing the RMS fluctuations of individual Cα atoms obtained from MD simulations of the native Cb with the corresponding values derived from the B−factors of the crystal structure, the values from the MD simulations are generally smaller. This result also indicates that the structure of the native Cb is relatively rigid. In artificial protein, the largest RMS fluctuations of Cα atoms show the residues on the open end of the four-helix bundle.